ChemComm

COMMUNICATION

View Article Online
View Journal | View Issue

Cite this: *Chem. Commun.*, 2015, **51**, 9030

Received 17th January 2015,
Accepted 8th April 2015

DOI: 10.1039/c4cc10399h

www.rsc.org/chemcomm

$NaYF_4$:Yb,Er–MoS_2: from synthesis and surface ligand stripping to negative infrared photoresponse†

Wenbin Niu,‡[ab] Hu Chen,‡[b] Rui Chen,[c] Jingfeng Huang,[b] Handong Sun[c] and Alfred Ling Yoong Tok*[b]

The synthesis, surface ligand stripping, and infrared optoelectronic device application of $NaYF_4$:Yb,Er–MoS_2 nanocomposites are reported. $NaYF_4$:Yb,Er–MoS_2 film shows an unusual negative infrared photoresponse after $SOCl_2$/DMF treatment, which exhibits more than two times the photoresponsivity of pure $NaYF_4$:Yb,Er, showing great potential for the development of novel infrared optoelectronic devices.

Nanocomposites have attracted great attention in recent years because of their composition-dependent properties.[1] Multicomponent nanomaterials containing two or more nanoscale components often exhibit multiple functionalities, and the interaction between the components in such systems may provide functionality that extends beyond those of the isolated materials. They may even exhibit novel properties, thus achieving potential applications in catalysis, optoelectronic and photovoltaic devices.[2] As a layered transition metal chalcogenide material, MoS_2 has shown great promise for its future electronic and catalytic applications by virtue of its unique structures, electrical and optical properties.[3] In particular, the direct band gap of mono- or few-layer MoS_2 suggests that it could be a promising material for optoelectronic applications.[4] For example, MoS_2 nanosheets exhibit a high channel mobility ($\sim$200 cm^2 V^{-1} s^{-1}), photoresponsivity (880 A W^{-1}) and current on/off ratio (10^{-8}) in a phototransistor.[4b,c] However, the current MoS_2 optoelectronic devices show low if not negligible photoresponsivity to light of wavelength >680 nm due to the weak absorption and intrinsic band gap of MoS_2 nanosheets.[4b–e] Therefore, it is essential to extend the photoresponse of devices to the long wavelength region, to broaden their applicability.

On the other hand, upconversion nanoparticles, particularly lanthanide-doped rare-earth nanocrystals, are capable of absorbing infrared irradiation and emit high-energy photons due to the special configuration of 4f electrons in rare-earth elements.[5] Among various upconversion materials, hexagonal $NaYF_4$:Yb,Er has been recognized as one of the most efficient UCNPs, showing potential applications in electronic devices, remote control devices and bioimaging.[2,6] However, studies on the nanocomposites of $NaYF_4$:Yb,Er and MoS_2 nanosheets for optoelectronic device applications are still absent so far. In this paper, we present the successful synthesis of $NaYF_4$:Yb,Er UCNPs–MoS_2 nanocomposites by a two-step thermolysis method in a mixture of oleic acid (OA) and oleylamine (OM) as described in the experimental section. A new method of $SOCl_2$/DMF treatment was then introduced to remove surface ligands of the as-prepared materials for optoelectronic device application (Scheme 1). Photoresponse measurements revealed that these devices exhibited unusual negative photoresponsivity to infrared light, and $NaYF_4$:Yb,Er UCNPs–MoS_2 demonstrated a negative photoresponsivity that was much higher than that of pure UCNPs.

Fig. 1 shows transmission electron microscopy (TEM) images of $NaYF_4$:Yb,Er UCNPs, MoS_2, and UNCPs–MoS_2 nanocomposites with a molar ratio of 1/0.2 of UNCPs/MoS_2. $NaYF_4$:Yb,Er UCNPs used for the synthesis of the nanocomposites were monodispersed in spherical shape with a size of around 16 nm as shown in Fig. 1a. The prepared pure MoS_2 was in a sheet nanostructure with few layers (Fig. 1b and Fig. S1, ESI†). Fig. 1c–e show typical TEM images of the obtained UCNPs–MoS_2 nanocomposites. It can be observed that UCNPs were anchored on MoS_2 nanosheets, and most of them were wrapped by loosely bound few-layered MoS_2 as indicated by arrows in Fig. 1c and d and Fig. S2 (ESI†). The average size of the $NaYF_4$:Yb,Er particles was slightly increased to $\sim$18 nm and some of them were in rod and irregular shapes with multicrystallites. This variation mainly resulted from Ostwald ripening and coalescence growth at high temperature during the synthesis

[a] *State Key Laboratory of Fine Chemicals, Dalian University of Technology, West Campus, 2 Linggong Rd., Dalian 116024, China*
[b] *School of Materials Science and Engineering, Nanyang Technological University, 50 Nanyang Avenue, 639798, Singapore. E-mail: MIYTok@ntu.edu.sg*
[c] *Division of Physics and Applied Physics, School of Physical and Mathematical Sciences, Nanyang Technological University, 21 Nanyang Link, 637371, Singapore*

† Electronic supplementary information (ESI) available: Experimental section, HRTEM of MoS_2, TEM, SEM and absorbance spectra of ligand-capped UCNPs–MoS_2 nanocomposites, upconversion spectra and TEM images of ligand-free UCNPs–MoS_2, upconversion mechanism and infrared photoresponse measurements of the nanocomposites. See DOI: 10.1039/c4cc10399h

‡ These authors contributed equally to this work.

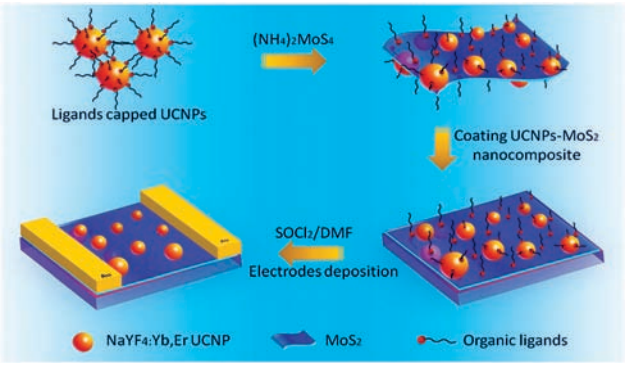

Scheme 1 Schematic illustration of the synthesis of $NaYF_4$:Yb,Er UNCPs–MoS_2 nanocomposites and the fabrication of photoresponse devices.

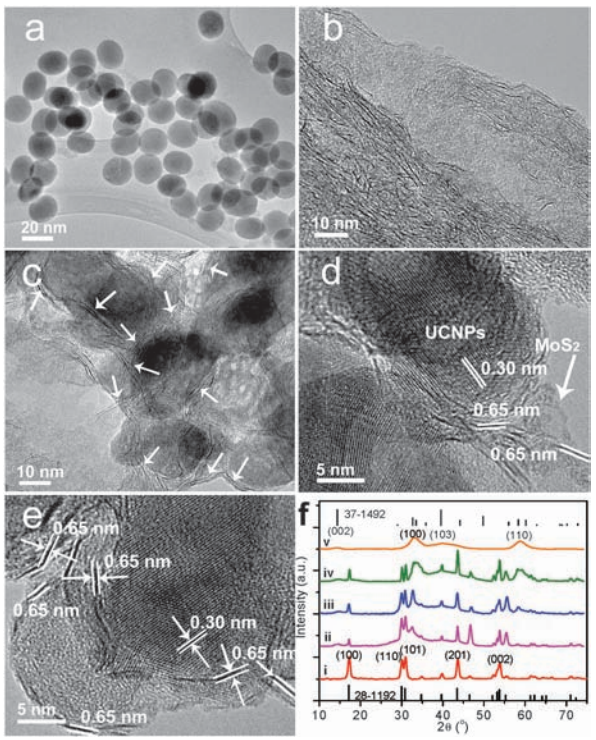

Fig. 1 TEM images of (a) $NaYF_4$:Yb,Er, (b) MoS_2, (c) $NaYF_4$:Yb,Er–MoS_2 (1/0.2), and (d, e) HRTEM images of the nanocomposites. (f) XRD patterns of (f-i) $NaYF_4$:Yb,Er, (f-v) MoS_2, and $NaYF_4$:Yb,Er–MoS_2 nanocomposites prepared with different molar ratios of UNCPs/MoS_2: (f-ii) 1/0.1, (f-iii) 1/0.2 and (f-iv) 1/0.4.

of the composites.[7] High resolution TEM (HRTEM) images (Fig. 1d and e) reveal lattice spacings of 0.3 and 0.65 nm, corresponding to the (110) facet of $NaYF_4$:Yb,Er and the (002) facet of the MoS_2 sheets, respectively, indicating the anchoring of UCNPs on MoS_2 nanosheets. As-prepared $NaYF_4$:Yb,Er–MoS_2 nanocomposites were also characterized by powder X-ray diffraction (XRD). The diffraction peaks and intensities of pure $NaYF_4$:Yb,Er (Fig. 1f-i) match well with the standard pattern of the hexagonal phase (JCPDS: 28-1192).[5,6] For pure MoS_2, there are the broadened peaks of the (101), (103) and (110) lattice planes (JCPDS: 37-1492),[8] while the peak of the (002) plane is weak, suggesting the predominant formation of few-layer MoS_2,[8] which agrees well with the TEM results. As for the UNCPs–MoS_2 composites, all samples showed the characteristic peaks of both $NaYF_4$:Yb,Er and MoS_2, and the peak intensities of MoS_2 [*e.g.* (100) and (110)] gradually increased with increasing MoS_2 ratio (Fig. 1f-i–iv). In addition, the relatively higher emission of a physical mixture of UCNPs and MoS_2 compared to their nanocomposite (Fig. S4, ESI†) further implies the close contact between $NaYF_4$:Yb,Er and MoS_2. Otherwise, the UCNPs–MoS_2 nanocomposite gave the same spectrum as that of their mixture (Fig. S4, ESI†). Furthermore, the excellent stability of the nanocomposites after surface ligand removal (discussed below) further implies a strong interaction between the UCNPs and the MoS_2 nanosheets. Therefore, in combination with the HRTEM images, XRD and upconversion spectra, these results indicate the formation of $NaYF_4$:Yb,Er–MoS_2 nanocomposites.

Fig. 2a shows the upconversion emission spectra of the corresponding samples. It can be clearly seen that the characteristic emission bands of the Er^{3+} ion were centred at 410, 520, 540 and 660 nm resulting from the $^4H_{9/2} \rightarrow {}^4I_{15/2}$, $^2H_{11/2} \rightarrow {}^4I_{15/2}$, $^4S_{3/2} \rightarrow {}^4I_{15/2}$ and $^4F_{9/2} \rightarrow {}^4I_{15/2}$ transitions, respectively. The composite samples show a reduction in emission intensity in comparison with pure $NaYF_4$:Yb,Er, and the intensity of the emission peaks decreased further with increasing amount of MoS_2 in the samples. This is because the strong absorption of MoS_2 at a broad wavelength range from 300 to 700 nm covers emissions of the $NaYF_4$:Yb,Er UCNPs (Fig. S5, ESI†). The reduced lifetime indicates the existence of fluorescence resonance energy transfer and/or charge transfer procedures in the nanocomposites (Fig. S6, ESI†). According to the data extracted, the energy transfer efficiency of the composite is determined to be around 0.16, indicating radiative energy transfer due to photon re-absorption also taking place.

In most cases, long hydrocarbon molecules containing a coordinating headgroup such as OA and OM were employed as surfactant ligands for the controlled synthesis and stabilization of high-quality nanomaterials. The presence of these large organic molecules, however, creates an insulating shell around the surface, thus blocking charge transport and limiting their applications in electronic and optoelectronic devices.[9] It is therefore necessary to remove these long-chain insulating ligands for practical device applications. In this work, a new approach for the removal of surface native ligands of as-prepared

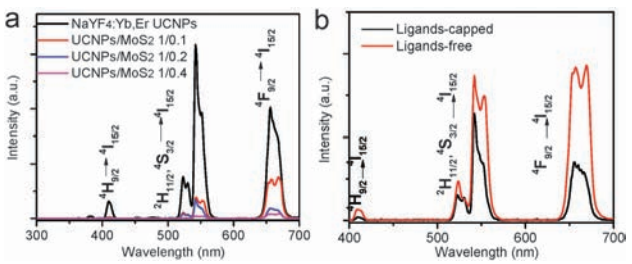

Fig. 2 Upconversion luminescence spectra of (a) $NaYF_4$:Yb,Er–MoS_2 composites with various molar ratios, and (b) $NaYF_4$:Yb,Er–MoS_2 (1/0.2) before and after ligand removal.

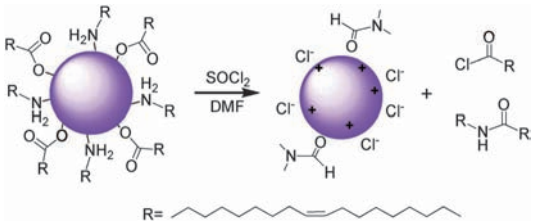

Scheme 2 Reactive ligand stripping of carboxylate- and amine-passivated nanomaterials with $SOCl_2$/DMF.

nanomaterials by $SOCl_2$/DMF (namely the Vilsmeier reagent) is also presented, which can be completed in 2 min. $SOCl_2$ is a well-known chloridization agent, and can readily react with carboxylic acids, amines, alcohols *etc.* DMF is used as a catalyst to activate $SOCl_2$ and accelerate the reaction with the surface ligands,[10] thus achieving rapid removal of the native ligands (Scheme 2). In the case that only $SOCl_2$ was added to the hexane dispersion of the nanoparticles, no apparent precipitation was found even after ultrasonication for several minutes. On the contrary, rapid precipitation of nanoparticles was observed after the addition of two drops of DMF with gentle shaking, indicating a dramatic change in material solubility as a result of the induced surface modification.

Fourier transform infrared (FT-IR) spectra of the samples (Fig. S7, ESI†) confirmed the removal of the surface ligands. As expected, all samples before $SOCl_2$/DMF treatment exhibited strong characteristic absorption bands of the alkyl chains of OA and OM (Fig. S7a–c, ESI†): the asymmetric and symmetric stretching vibrations of methylene (CH_2 at 2924 and 2853 cm^{-1}) and carboxyl groups (COO^-) at around 1564 cm^{-1}.[11] After treatment with $SOCl_2$/DMF, these signals were absent, confirming complete removal of organic surfactants from the nanomaterial surface. The resulting precipitate can be well redispersed in polar solvents such as DMF and DMSO (Fig. S8a–c, ESI†). Fig. S8d–f (ESI†) exhibit the corresponding TEM images. For the UCNPs, their size and shape were preserved after treatment, and no obvious aggregation was observed upon surface modification (Fig. S7, ESI†). The shape of the MoS_2 was slightly changed after treatment, and no initially loose layers were shown (Fig. S8e and S9, ESI†). Notably, the removal of organic ligands led to the variation in upconversion emission. For example, compared to the untreated $NaYF_4$:Yb,Er–MoS_2 composite (1/0.2), all emission intensities of the $^4H_{9/2} \rightarrow {}^4I_{15/2}$, $^2H_{11/2}$, $^4S_{3/2} \rightarrow {}^4I_{15/2}$ and $^4F_{9/2} \rightarrow {}^4I_{15/2}$ transitions in the modified composites were much higher (Fig. 2b). This is because the removal of organic ligands with long alkyl chains reduces the nonradiative relaxation of excited Er^{3+} ions from $^2H_{11/2}$/$^4S_{3/2}$ to $^4F_{9/2}$ and $^4I_{11/2}$ to $^4I_{13/2}$ levels (Fig. S10, ESI†),[11] thus enhancing emission intensities. The successful stripping and redispersion of UCNPs, MoS_2 nanosheets and their composites passivated by either oleate or amine ligands imply the potential applications of this method for a variety of nanocrystals with different sizes, shapes, and surface ligands. Instead of the tetrafluoroborates and metal chalcogenide complexes reported before,[9,12] readily available $SOCl_2$/DMF is employed in this work, which was demonstrated to be a facile, rapid and efficient approach for the removal of native ligands while leaving the surface of the nanomaterial bare and hydrophilic.

To demonstrate infrared photodetector applications, photoresponse devices with the corresponding materials were fabricated. The photoresponses of these devices upon 980 nm infrared light irradiation were investigated. For the device fabrication, the films of the surfactant ligand-capped nanomaterials were deposited on substrate, followed by immersion in a dilute solution of $SOCl_2$/DMF in hexane to remove the insulating organic ligands. Lastly, gold electrodes were deposited on top. Due to the efficient removal of the insulating ligands, a favorable effect on the optoelectronic properties of the treated films was anticipated. Fig. 3a shows the time-dependent normalized drain current of the devices with a source–drain voltage (V_{DS}) of 10 mV at zero gate bias. Importantly, different from the usually-observed positive photocurrent response in semiconductor nanomaterials, an unexpected *negative* photoresponse was exhibited by their films upon 980 nm infrared light irradiation (Fig. 3a, Fig. S11 and S12, ESI†). Once the incident light was removed, the current jumped back to the baseline level. Specifically, the photoresponse device with pure UCNPs exhibited a 30% decrease in I_d. For the UCNP–MoS_2 nanocomposites, the device with a UCNP/MoS_2 ratio of 1/0.1 exhibited a 50% decrease in source–drain current, and the one with a molar ratio of 1/0.2 showed up to a 75% decrease (Fig. 3a), while no source–drain current was measured for the 1/0.4 nanocomposite or pure MoS_2, due to the large cracks induced by the reduction of the inter-nanosheet spacing after $SOCl_2$/DMF treatment (Fig. S13, ESI†).[12a] It was indicated that the presence of MoS_2 in the nanocomposites led to a stronger negative photoresponse; however, an excess amount of MoS_2 resulted in the formation of large cracks in the films after $SOCl_2$/DMF treatment and as a result, no source–drain current was measured.

Recently, Talapin *et al.* proposed a model to explain the negative photoconductivity in InAs nanocrystal film,[9c] in which a donor-like state forms a localized level (D_{ss}) presumably located above the mobility edge. Photo-induced trapping of mobile electrons in this localized level (D_{ss}) resulted in negative photoconductivity. Such a donor-like surface state has been observed in semiconductor nanocrystals.[13] This model is also a

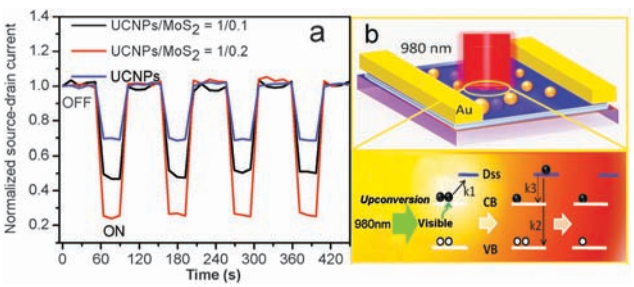

Fig. 3 (a) Real-time measurements of the normalized drain current of the infrared photoresponse devices while the 980 nm infrared light is switched on and off with V_{DS} of 10 mV at zero gate bias. UCNPs and UCNPs/MoS_2 (1/0.1 and 1/0.2) represent the devices prepared with $NaYF_4$:Yb,Er UCNPs and $NaYF_4$:Yb,Er–MoS_2 composite (1/0.1, 1/0.2) films treated with a hexane solution of $SOCl_2$/DMF. (b) Schematic illustration of the device and the proposed mechanism of negative infrared photoresponse.

reasonable explanation for the experimentally observed negative photoresponses in this work (see ESI† for more details). We presume that the donor-like surface state is also formed in UCNPs and MoS_2 after surface treatment and located above the mobility edge (Fig. 3b). Upon 980 nm irradiation, a mobile electron is excited and becomes trapped at the D_{ss} level (k1), resulting in decreased conductivity. The electron trapped in the D_{ss} state can either nonradiatively recombine with a hole in the valence band (k2, VB) or relax into the conduction band (k3, CB). When the infrared light is off, electrons are no longer trapped and the conductivity is restored. Increasing the ratio of MoS_2 in the hybrid composites may increase the D_{ss} surface state due to the large specific area of the nanosheet structure, thus causing a stronger negative photoresponse. The detailed mechanism is still under investigation.

In summary, the synthesis, surface ligand stripping, and negative infrared photoresponse of new $NaYF_4$:Yb,Er UCNPs–MoS_2 nanocomposites were demonstrated. The synthesis of the composites was achieved by a thermolysis method in organic surfactant ligands. We then presented a new method using $SOCl_2$/DMF treatment to remove surface ligands of these nanomaterials for device applications, which was demonstrated to be a facile, rapid yet efficient approach for the complete removal of native ligands, showing potential applications for a variety of nanocrystals. Most importantly, after $SOCl_2$/DMF treatment, the UCNPs–MoS_2 nanocomposite films exhibited unexpected negative photoresponses to 980 nm illumination, and the photoresponsivity of UCNPs–MoS_2 (1/0.2) was more than two times that of pure UCNPs, indicating potential application of these materials in infrared photoresponse devices. Also, this negative photoresponse phenomenon provides the opportunity for the development of novel optoelectronic devices.

Notes and references

1 (*a*) A. G. Dong, J. Chen, P. M. Vora, J. M. Kikkawa and C. B. Murray, *Nature*, 2010, **466**, 474; (*b*) P. Li, Z. Wei, T. Wu, Q. Peng and Y. D. Li, *J. Am. Chem. Soc.*, 2011, **133**, 5660.

2 L. Cheng, K. Yang, Y. G. Li, J. H. Chen, C. Wang, M. W. Shao, S. T. Lee and Z. Liu, *Angew. Chem., Int. Ed.*, 2011, **50**, 7385.

3 (*a*) F. K. Meng, J. T. Li, S. K. Cushing, M. J. Zhi and N. Q. Wu, *J. Am. Chem. Soc.*, 2013, **135**, 10286; (*b*) Q. J. Xiang, J. G. Yu and M. Jaroniec, *J. Am. Chem. Soc.*, 2012, **134**, 6575; (*c*) J. Yang, D. Voiry, S. J. Ahn, D. Kang, A. Y. Kim, M. Chhowalla and H. S. Shin, *Angew. Chem., Int. Ed.*, 2013, **52**, 13751.

4 (*a*) M. Chhowalla, H. S. Shin, G. Eda, L. J. Li, K. P. Loh and H. Zhang, *Nat. Chem.*, 2013, **5**, 263; (*b*) O. Lopez-Sanchez, D. Lembke, M. Kayci, A. Radenovic and A. Kis, *Nat. Nanotechnol.*, 2013, **8**, 497; (*c*) Z. Y. Yin, H. Li, H. Li, L. Jiang, Y. M. Shi, Y. H. Sun, G. Lu, Q. Zhang, X. D. Chen and H. Zhang, *ACS Nano*, 2012, **6**, 74; (*d*) S. H. Su, Y. T. Hsu, Y. H. Chang, M. H. Chiu, C. L. Hsu, W. H. Chang, J. H. He and L. J. Li, *Small*, 2014, **10**, 2589.

5 (*a*) L. Cheng, C. Wang, X. X. Ma, Q. L. Wang, Y. Cheng, H. Wang, Y. G. Li and Z. Liu, *Adv. Funct. Mater.*, 2013, **23**, 272; (*b*) D. Chen, Y. Yu, F. Huang, A. Yang and Y. S. Wang, *J. Mater. Chem.*, 2011, **21**, 6186; (*c*) F. Wang and X. G. Liu, *J. Am. Chem. Soc.*, 2008, **130**, 5642; (*d*) X. J. Xie, N. Y. Gao, R. R. Deng, Q. Sun, Q. H. Xu and X. G. Liu, *J. Am. Chem. Soc.*, 2013, **135**, 12608; (*e*) D. Li, Q. Shao, Y. Dong and J. Jiang, *Chem. Commun.*, 2014, **50**, 15316; (*f*) Z. Yin, Y. Zhu, W. Xu, J. Wang, S. Xu, B. Dong, L. Xu, S. Zhang and H. Song, *Chem. Commun.*, 2013, **49**, 3781; (*g*) Y. S. Liu, D. T. Tu, H. M. Zhu, R. F. Li, W. Q. Luo and X. Y. Chen, *Adv. Mater.*, 2010, **22**, 3266; (*h*) N. Bogdan, F. Vetrone, G. A. Ozin and J. A. Capobianco, *Nano Lett.*, 2011, **11**, 835; (*i*) F. Wang, L. D. Sun, J. Gu, Y. F. Wang, W. Feng, Y. Yang, J. F. Wang and C. H. Yan, *Angew. Chem., Int. Ed.*, 2012, **51**, 8796; (*j*) W. B. Niu, L. T. Su, R. Chen, H. Chen, Y. Wang, A. Palaniappan, H. D. Sun and A. L. Y. Tok, *Nanoscale*, 2014, **6**, 817.

6 (*a*) B. Dong, S. Xu, J. Sun, S. Bi, D. Li, X. Bai, Y. Wang, L. Wang and H. Song, *J. Mater. Chem.*, 2011, **21**, 6193; (*b*) Y. Liu, M. Chen, T. Y. Cao, Y. Sun, C. Y. Li, Q. Liu, T. S. Yang, L. M. Yao, W. Feng and F. Y. Li, *J. Am. Chem. Soc.*, 2013, **135**, 9869; (*c*) C. L. Zhang, Y. X. Yuan, S. M. Zhang, Y. H. Wang and Z. H. Liu, *Angew. Chem., Int. Ed.*, 2011, **50**, 6851; (*d*) Z. Y. Hou, C. X. Li, P. A. Ma, G. G. Li, Z. Y. Cheng, C. Peng, D. M. Yang, P. P. Yang and J. Lin, *Adv. Funct. Mater.*, 2011, **21**, 2356; (*e*) W. Li, J. S. Wang, J. S. Ren and X. G. Qu, *J. Am. Chem. Soc.*, 2014, **136**, 2248; (*f*) Y. L. Dai, H. H. Xiao, J. H. Liu, Q. H. Yuan, P. A. Ma, D. M. Yang, C. X. Li, Z. Y. Cheng, Z. Y. Hou, P. P. Yang and J. Lin, *J. Am. Chem. Soc.*, 2013, **135**, 18920; (*g*) S. Wang, L. Zhang, C. Dong, L. Su, H. Wang and J. Chang, *Chem. Commun.*, 2015, **51**, 406; (*h*) Q. Kong, L. Zhang, J. Liu, M. Wu, Y. Chen, J. Feng and J. Shi, *Chem. Commun.*, 2014, **50**, 15772; (*i*) Y. Wu, Y. Cen, L. Huang, R. Yu and X. Chu, *Chem. Commun.*, 2014, **50**, 4759; (*j*) J. Chang, Y. Ning, S. Wu, W. Niu and S. Zhang, *Adv. Funct. Mater.*, 2013, **23**, 5910.

7 (*a*) N. J. J. Johnson, A. Korinek, C. H. Dong and F. C. J. M. van Veggel, *J. Am. Chem. Soc.*, 2012, **134**, 11068; (*b*) X. C. Ye, J. E. Collins, Y. J. Kang, J. Chen, D. T. N. Chen, A. G. Yodh and C. B. Murray, *Proc. Natl. Acad. Sci. U. S. A.*, 2010, **107**, 22430; (*c*) H. Zheng, R. K. Smith, Y. Jun, C. Kisielowski, U. Dahmen and A. P. Alivisatos, *Science*, 2009, **324**, 1309.

8 C. Altavilla, M. Sarno and P. Ciambelli, *Chem. Mater.*, 2011, **23**, 3879.

9 (*a*) M. V. Kovalenko, M. Scheele and D. V. Talapin, *Science*, 2009, **324**, 1417; (*b*) D. S. Chung, J. S. Lee, J. Huang, A. Nag, S. Ithurria and D. V. Talapin, *Nano Lett.*, 2012, **12**, 1813; (*c*) W. Y. Liu, J. S. Lee and D. V. Talapin, *J. Am. Chem. Soc.*, 2013, **135**, 1349.

10 (*a*) A. Arrieta, J. M. Aizpurua and C. Palomo, *Tetrahedron Lett.*, 1984, **25**, 3365; (*b*) F. Xu, B. Simmons, R. A. Reamer, E. Corley, J. Murry and D. Tschaen, *J. Org. Chem.*, 2008, **73**, 312.

11 (*a*) W. B. Niu, S. L. Wu and S. F. Zhang, *J. Mater. Chem.*, 2011, **21**, 10894; (*b*) W. B. Niu, S. L. Wu, S. F. Zhang, J. Li and L. Li, *Dalton Trans.*, 2011, **40**, 3305.

12 (*a*) E. L. Rosen, R. Buonsanti, A. Llordes, A. M. Sawvel, D. J. Milliron and B. A. Helms, *Angew. Chem., Int. Ed.*, 2012, **51**, 684; (*b*) A. G. Dong, X. C. Ye, J. Chen, Y. J. Kang, T. Gordon, J. M. Kikkawa and C. B. Murray, *J. Am. Chem. Soc.*, 2011, **133**, 998; (*c*) S. D. Dmitry, N. Dirin, M. I. Bodnarchuk, G. Nedelcu, P. Papagiorgis, G. Itskos and M. V. Kovalenko, *J. Am. Chem. Soc.*, 2014, **136**, 6550.

13 (*a*) M. Shim and P. Guyot-Sionnest, *Nature*, 2000, **407**, 981; (*b*) D. Y. Petrovykh, M. J. Yang and L. J. Whitman, *Surf. Sci.*, 2003, **523**, 231.